Generation and characterization of white-light continuum in a microstructure fiber

Daniel Burke

Adviser: Jan Chaloupka

1.0 Background and Theory

White-light continuum generation is a fascinating phenomenon in nonlinear optics, in which the narrow bandwidth of a quasimonochromatic light pulse is broadened by self-phase modulation (SPM) in a nonlinear medium. SPM involves characteristics of both the medium and the light pulse itself as opposed to processes such as fluorescence and the spontaneous Raman effect that involve the energy levels of a material. Such processes also generate wider output bandwidths and have been investigated in great detail [1]. Figure 1a shows traditional Rayleigh scattering, in which a particle absorbs a photon, enters an excited state, and then emits a photon of the same energy, dropping back to its original state. Fluorescence (Figure 1b) occurs when a particle absorbs a photon and enters an excited energy state. The particle then releases a photon of a lower energy, dropping to a higher state. The differences between the initial and final energy states are known as Stokes transitions. The spontaneous Raman effect (Figure 1c), discovered in 1928, is similar to the process of fluorescence. In this case, after a particle absorbs a photon, it emits a photon of even higher energy and drops to a state even lower than its initial state. The differences between these two energy levels are called anti-Stokes transitions.

With the development of the ultrafast laser, scientists can create light at intensities high enough to examine nonlinear optical effects, such as harmonics generation, self-focusing, and SPM [1]. SPM is related to the Kerr effect, in which a medium's index of refraction is affected by an electric field. In SPM, the change in the index of refraction is caused by

the electric field of a photon in the medium [2]. All optical media will exhibit SPM at high enough intensities.

Optical fibers have been used to investigate nonlinear optics within the past forty years [3]. Several types of fibers are already in widespread use. Standard optical fibers, such as those used for telecommunications and computing, consist of a solid silica core surrounded by a cladding. Light is transmitted through the length of the fiber via total internal reflection due to the index of refraction difference between the core and the cladding. Microstructure (MS) fibers have become the subject of significant research within the past decade. Compared to ordinary fibers, MS fibers exhibit extraordinary properties such as a high nonlinear index of refraction and low dispersion [4, 5]. MS fibers usually consist of a solid core surrounded by a hexagonal lattice of small air holes that run the length of the fiber [5]. Latest research of the nonlinear characteristics of MS fibers shows applications in medical imaging [4], quantum computing [6], and white-light continuum generation [7].

SPM has been treated theoretically by several authors [3, 8, 9]. SPM assumes a nonlinear index of refraction that can be written as:

$$n = n_0 + n_2 I(z,t) \quad (1),$$

where n_o is the linear index of refraction and $I(z, t)$ is the intensity function. The nonlinear constant, n_2, can be directly measured [10]. A time-independent Gaussian pulse envelope traveling in the z-direction can be defined as:

$$E(z,0) = E_0 \exp\left[\frac{-1}{2}\left(\frac{z}{z_0}\right)^2\right] \quad (2),$$

where z_0 is constant defined by the width of the pulse. Cheung notes a frequency shift given a quasimonochromatic pulse of frequency ω_0, traveling through length L of fiber, and intensity dependent index of refraction [9]:

$$\Delta\omega = \omega_0\left(\frac{n_2 L}{n}\right)\frac{\partial}{\partial z}E(z,0)^2 \quad (3).$$

Differentiating the above equation with respect to z and solving for the extrema, we can approximate a maximum shift in bandwidth on both edges of the pulse:

$$\Delta\omega_{\max} \approx \pm\frac{\sqrt{2}}{2}\frac{\omega_0 L}{n_0} z_0 E_0^2 \quad (4).$$

The frequency spectrum of the output pulse can be thought of as consisting of frequencies ranging from $\omega_0 - \Delta\omega_{max}$ to $\omega_0 + \Delta\omega_{max}$. Figure 2 demonstrates this shift in frequency on a Gaussian pulse envelope. Since the index of refraction is intensity dependent, different parts of the pulse envelope travel at different speeds in the medium. The center of the pulse, having the highest intensity, travels slower than the leading and trailing edges. This results in a reshaping, or self-steepening of the pulse [2, 8]. With Mathcad, a simple simulation of this effect was designed by graphing a Gaussian envelope for a pulse given by Equation 2. The pulse's movement through a nonlinear medium was simulated by translating each point on the graph. The magnitude of each translation was defined by multiplying an arbitrary amount of time by an intensity dependent velocity. Figure 3 shows several frames of the pulse undergoing SPM in an optical fiber. While this does demonstrate the effect of the pulse reshaping, it does not account for the discontinuity in the trailing edge of the pulse. DeMartini notes that dispersion in the medium prevents the

pulse from becoming infinitely steep on the trailing edge [8]. Figure 4 shows the same frames as figure 3 with simulated optical cycles under the envelope. To simulate the optical cycles, the intensity $E(r)^2$ term was multiplied by an arbitrary sinusoidal function. As the pulse travels through the medium, the wavelengths at the front of the pulse get longer, corresponding to a decrease in frequency. The wavelengths at the trailing end of the pulse get shorter, corresponding to an increase in frequency. These spectral shifts qualitatively agree with equation 3. Some graphs that incorporate the Fourier frequency transforms of the pulses were designed (figures 5 and 6). While these graphs do not truly represent SPM, they do demonstrate how the bandwidth of a pulse is broadened by the nonlinear index of refraction. Figure 5 shows the simulated frequency spectra for pulses of different lengths. Shorter pulses require wider bandwidths, which can be seen in figure 5, verifying the simulations. Figure 6 shows different levels of distortion on pulses and the respective frequency spectra. As the pulse is distorted more, the frequency spectrum gets broader, resulting in more peaks. Cheung gives the Fourier frequency spectrum $S(L, \omega)$ for a pulse traveling a distance L in an optical fiber [9]:

$$S(L, \omega) = (cn/8\pi) \mid E(L, \omega) \mid^2 \quad (5).$$

Given a high enough nonlinear constant, the bandwidth can be widened so that the output is a white-light continuum over the visual spectrum.

2.0 Experiment

The goal of this project was to generate a white-light continuum and to characterize continuum output from a Ti:sapphire laser through a length of MS fiber. Before any characterization could be done, methods of properly cleaving the fiber had to be learned.

Several weeks were spent investigating various methods of cleaving the optical fiber. As the MS fiber is expensive, the methods were practiced on a standard fiber from Thor Labs. The fiber consists of a solid silica core with a diameter of approximately 125 μm surrounded by a cladding with a diameter of 250 μm. Using a specially designed fiber optic stripper from Clauss, the cladding was removed from the fiber. Once several lengths of fiber had been successfully stripped, the fiber was cleaved using various tools in the lab. Figure 7 shows several end faces cut using different methods. These included snapping the fiber by hand (7a), cutting the fiber with a pair of scissors (7b), scoring the fiber with a diamond tipped tool from Fiber Instrument Sales (7c), and using an optical fiber cleaver from FITEL (7d). The end faces of the fiber were photographed using a digital microscope from Motic. Of the methods tried, the FITEL cleaver worked the best, yielding clean faces on the input and output ends of the fiber.

Some problems arose in trying to cleave the fiber. One problem was the fiber stripping tool. During the course of removing the cladding from the fiber, the tool left tiny score marks along the length of the fiber (see Figure 8). As these score marks would affect the propagation through the fiber, extra care was needed while stripping the fiber. Another problem was the consistency in which the fiber could be cleaved successfully. A significant portion of the standard fiber had to be discarded in order to get clean input and output faces. As a large supply of the standard fiber was available, this was not a problem. However, the supply of the MS fiber was limited to a short piece of about 8 cm, meaning that there were only a few chances to get a decent cut. Having found the best method of cleaving the fiber, an apparatus was devised to measure the output from

the MS fiber. Figure 9 shows the apparatus used. The apparatus consisted of a Helium-Neon laser from Coherent with a maximum output of 10mW at a wavelength of 632.8 nm. This laser was mounted on a 12" by 24" by 0.5" breadboard from Thor Labs. The laser beam was aligned with a pair of gold mirrors, using two irises to define the z-axis of the experiment. A Thor Labs lens with an effective focal length of 3.1 mm was placed along this axis, followed by a fiber chamber. The lens was mounted on a Newport stand with actuators that allowed for movement in the perpendicular x and y directions. The fiber was mounted on a similar stand with movement in all three directions. A second lens with a focal length of approximately 10 cm was mounted after the fiber. This second lens collimated the output from the fiber and focused it to a point at the end of the breadboard to a Thor Labs PIN diode connected to a digital multimeter. A neutral density filter was placed between the second lens and the PIN diode so that the diode did not saturate.

The PIN diode setup allowed me to make relative measurements of the output from the fiber. A piece of fiber with a length of approximately 2 cm was placed into the fiber chamber and the actuators adjusted so that the output from the fiber on the PIN diode was maximized. Once a reading was obtained from the multimeter, the fiber chamber was removed and replaced with the first lens. Because the lens has a focal length much shorter than the fiber, the lens had to be positioned so that the laser spot would focus on the PIN diode. The position of the first lens was adjusted so that the output on the PIN diode was maximized. This process was repeated several times in the hope of getting a

consistent ratio of output with fiber in place versus output without the fiber. Percent loss was calculated by the following formula:

$$\%Loss = \left(1 - \frac{V_{fiber}}{V_{nofiber}}\right) * 100 \quad (6)$$

where V is the maximum DC voltage reading of the multimeter. Initial measurements of loss were inconsistent. For three similar lengths of fibers, losses of 30%, 57%, and 82% were measured. The inconsistency of these measurements demonstrated that something about the apparatus was wrong. First, the stands holding the fiber and the first lens were switched. This allowed for more flexibility in positioning the second lens. Then, a smaller lens with a much shorter focal length (f ~ 8mm) that could focus the output beam onto the PIN diode was obtained. This lens was mounted on a third stand, so its positioning could be more precise. Then, the neutral density filters were verified. These filters are designed to transmit a small percentage of an incident beam. The fraction of transmitted power, T, is given by $T = 10^{-D}$, where D is the optical density. As a way of checking the validity of my apparatus, the experiment was run again, but with varying optical density of the filters. The PIN diode saturated at 12V; however, for readings less than this value, the readings matched the expected exponential curve. Using the measured voltages, the expected values were extrapolated beyond the saturation of the PIN diode and got an exponential curve consistent with the equation for transmitted power. Figure 10 shows the measured voltage values and the extrapolated curve as a function of optical density D.

The apparatus was then adapted for use with the Ti:sapphire laser. Figure 11 shows a diagram of the apparatus used. The same Newport mounts were used. The input beam

was directed through a pair of prisms; this technique has been shown to be an effective method to compensate for dispersion [11]. The primary axis of the experiment was defined with a pair of irises and positioned the lens and fiber mounts as before. A length of the standard fiber (L ~ 85cm) was cut and the input end was placed in the fiber chamber. A different lens (f ~ 8mm) was used to focus the laser beam into the fiber. Figure 12 shows the input and output faces of the fiber used. The input beam was measured with a spectrometer. Rather than collimate the output with a second lens, the output beam was directed to a spectrometer. With this apparatus, the input spectrum and the output spectrum were compared given different input settings. First, the input power was measured and compared to the output power. Then, the input power was varied by placing a series of neutral density filters in front of the lens and taking the output spectrum for each setting. The spectra for different input wavelengths from the Ti:sapphire laser were taken.

3.0 Data and Analysis

Initially, an input power of 380mW was measured compared to an output power of 140mW. This translates to a 63% loss of power through the fiber. This loss is less than the measured loss of the He-Ne laser of 76%. This loss is due to several factors. Since there is no anti-reflective coating on the fiber, some of the light is reflected back off the input face of the fiber. Another possible source of loss is a mismatch of numerical apertures (NA). A difference of NA will result in a portion of the input light not coupling into the fiber. The specific value of the NA for the fiber used is uncertain, but according to Thor Labs, a typical standard fiber has a numerical aperture of 0.13. A laser spot

diameter of 2mm through a lens with a focal length of 8mm gives a numerical aperture of 0.12. These values are fairly close, so the loss due to mismatched NA is minimal. Some light was also lost through the bends of the fiber (see Figure 13). Finally, the focusing of the beam is not perfect, so not all of the light was coupled into the fiber.

Figure 14 shows the spectra for different power levels. Since the change in frequency is dependent on the input intensity, a smaller spectral shift is expected for lower power input. Figure 14a shows the input (red) and output (blue) spectra for an input power of 380mW, 14b at 300mW, 14c at 160mW, 14d at 110mW, 14e at 63mW, and 14f at 50mW. At the highest power setting, the bandwidth is widest; at the lowest power setting, the output spectrum closely resembles the input. The graph in figure 15 shows that as the input power increases, the output spectra bandwidth widens. The input has a narrow bandwidth of about 40nm (FWHM), centered at 835nm. When the laser is at full power, the spectrum bandwidth is broadened to 66nm. At low power, the bandwidth reduces to 43nm. These results qualitatively agree with what was expected, given the intensity dependent index of refraction. According to equation 4, the maximum spectral shift is linear with intensity. The bandwidth at FWHM does closely follow a linear fit, as the trend line in figure 13 shows, with an R^2 value of 0.9696. A slight spectral shift was also observed, as the output spectrum was centered at 820nm. Since the fiber does not transmit light equally well for all colors, a spectral shift can be seen at low intensities. Observations show that our fiber is more efficient at transmitting visible light rather than IR. As the pulses travel through the fiber, longer wavelengths are slightly attenuated, resulting in the spectral shift seen.

Attempts to change the wavelength provided some interesting results. Figure 16 shows various input spectra along with the respective fiber output spectra. Figure 16a shows the same SPM effects as figure 14a, with the input spectrum centered at 835nm. When the input wavelength was shifted toward the blue end of the spectrum, the fiber spectrum gave a sharp spike at the 770nm (see figure 16b). This spike represents a continuous wave component of the input, as the laser went out of mode-lock when we tried to shift the frequency further. This is a surprising discovery, as the input spectrum for this setting shows no sign of going out of mode-lock. We are intrigued that the observation of the SPM-modified spectrum could be used as a precursor to detect when the mode-locking in the laser oscillator is about to fail, as this spectrum shows the CW component much more strongly. Figure 16c shows an input spectrum at 882nm with two peaks on the output spectrum at 857nm and 872nm. It is fascinating that even with such a seemingly simple interaction, namely ultrashort laser pulses in an ordinary optical fiber, that there is evidence of such rich behavior. A more complete analysis of this structured output, perhaps with a full temporal characterization, would help us to better understand the nonlinear interaction.

4.0 Conclusion

There are numerous opportunities for further research in this field. Given the high intensity capability of the Ti:sapphire laser, a future student could investigate the effects of SPM without the MS fiber. For example, further investigation is needed of the dependence of the output spectrum on the input wavelength. Another interesting

measurement to look at would be the spatial distribution of the output pulse. Since the output of the fiber diverges rapidly from the end face, the spectrometer was only able to measure a small portion of the output. Also, more rigorous computer simulations of the pulse reshaping that include full Fourier analysis of the output pulses would provide more insight into the effects of SPM.

Working with the MS fiber proved to be difficult, especially since a limited supply of the fiber was available. Given more fiber with which to experiment, the student could better demonstrate the nonlinear properties of the MS fiber. Consistent cleaving of the MS fiber is one skill that needs to be mastered before any further experiments can take place. Once the white-light continuum is generated, the student could vary the input beam and examine how differences in the beam affect the output bandwidth and try to characterize the output pulses.

Throughout this project, the phenomenon of SPM was investigated with computer simulations and experiments. The spectral broadening was witnessed through the ordinary fiber and measured at varying intensities, confirming the theory that has been developed. We also discovered some surprising effects of SPM that should be investigated further, such as the effect of input spectra on the output. While we were not able to observe the white-light continuum output, we have developed tools useful for future work.

5.0 References

1. E. Hecht, *Optics 4th Ed* (Addison Wesley, 2002)
2. T. K. Gustafson, J. P. Taran, H. A. Haus, J. R. Lifsitz, and P. L. Kelley, Phys. Rev. **177**, 303 (1969).
3. E. P. Ippen, C. V. Shank, and T. K. Gustafson, Appl. Phys. Lett. **24**, 190 (1974).
4. T. M. Fortier, S. T. Cundiff, I. T. Lima, Jr., B. S. Marks, C. R. Menyuk, and R. S. Windeler, Opt. Lett. **29**, 21 (2004).
5. C. Zhang, G. Kai, Z. Wang, T. Sun, C. Wang, Y. Liu, W Zhang, J. Liu, S. Yuon, and X. Dong, Opt. Lett. **30**, 18 (2005).
6. J. Fan, A. Dogariu, and L. J. Wang, Opt. Lett. **30**, 12 (2005).
7. X. Gu, L. Xu, M. Kimmel, E. Zeek, P. O'Shea, A. P. Shreenath, R. Trebino, and R. S. Windeler, Opt. Lett. **27**, 13 (2002).
8. F. DeMartini, C. H. Townes, T. K. Gustafson, and P. L. Kelley, Phys. Rev. **164**, 312 (1967).
9. A. C. Cheung, D. M. Rank, R. Y. Chiao, and C. H. Townes, Phys. Rev. Lett. **20**, 786, (1968).
10. A. J. Taylor, G. Rodriguez, T. S. Clement, Opt. Lett. 21, 1812, (1996).
11. S. Yang, K. Lee, Z. Xu, X. Zhang, and X. Xu, Opt. and Lasers in Eng. **36**, 381 (2001).

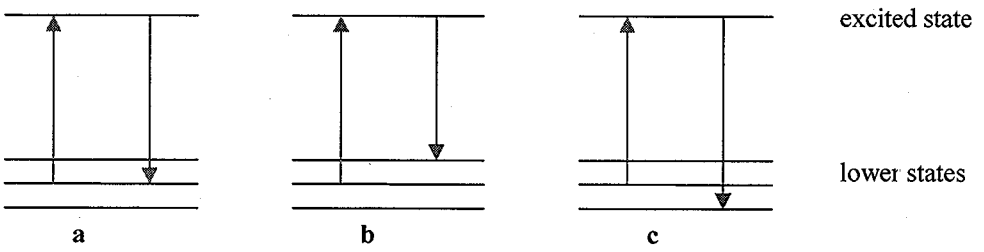

Figure 1: a) Traditional Rayleigh scattering. The particle absorbs a photon and releases a photon of the same energy, dropping back to the same initial state. b) Fluorescence. The particle absorbs a photon and releases a photon of lower energy, dropping to a state higher than its initial state. c) Raman shift. The particle absorbs a photon and releases a photon of higher energy, dropping to a state lower than its initial state [1].

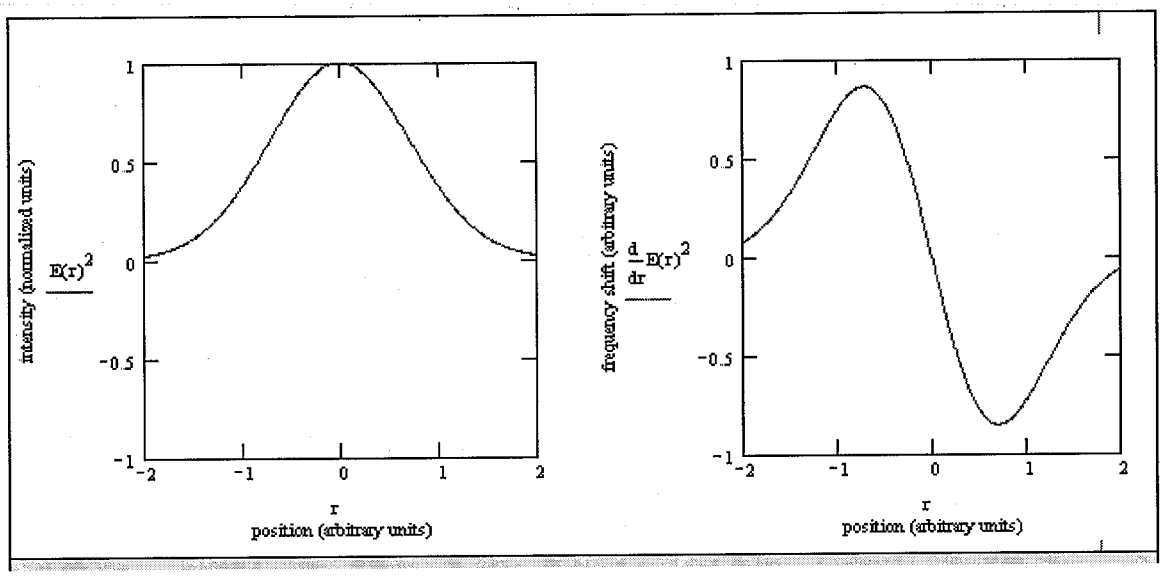

Figure 2: Gaussian pulse and frequency shift. The first graph represents a Gaussian laser pulse traveling in one arbitrary dimension r. The second graph represents a frequency shift given by equation 4 on both the leading and trailing edges of the pulse after it has undergone SPM.

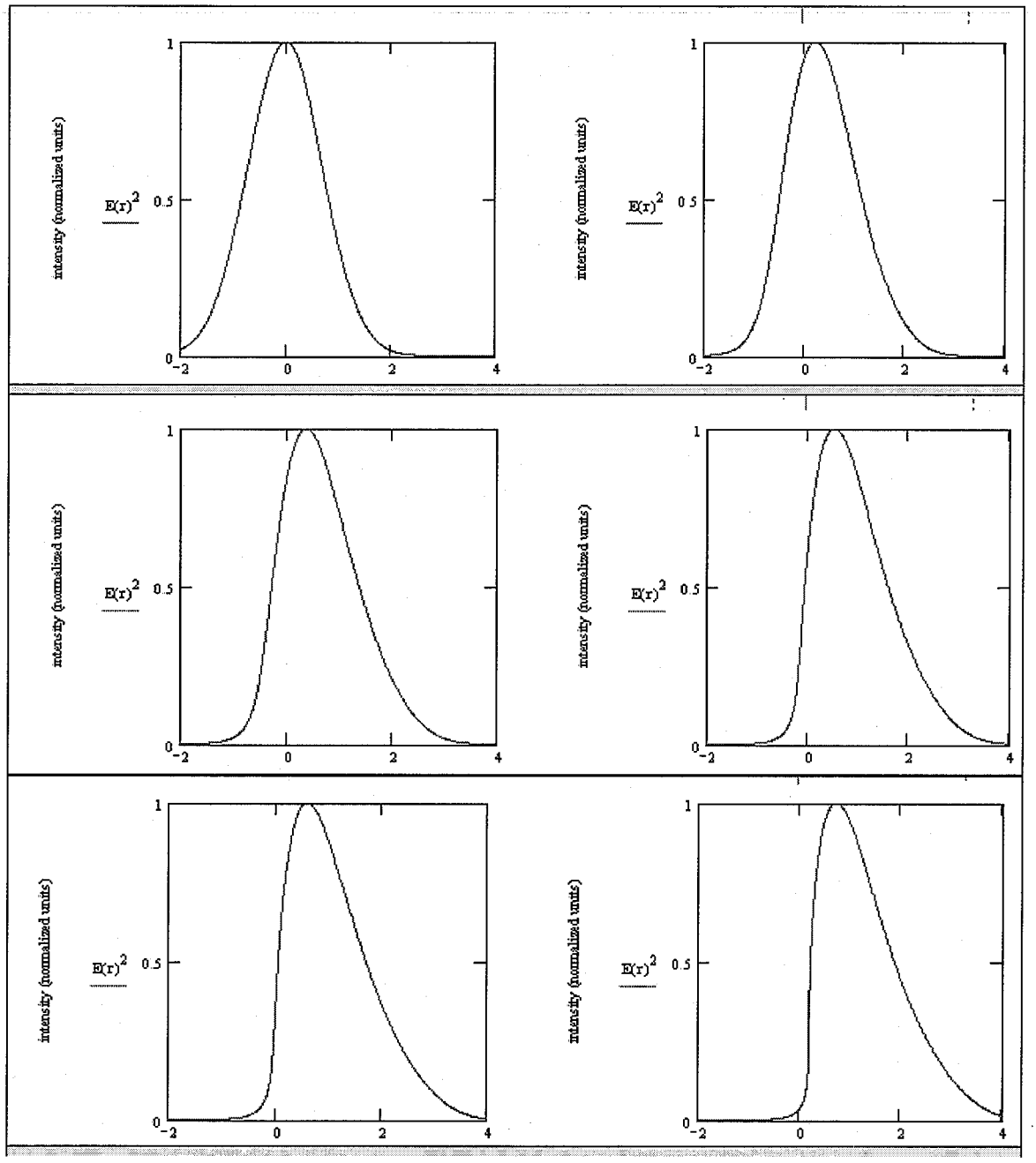

Figure 3: Gaussian pulse reshaping. These frames demonstrate a Gaussian envelope given by equation 2 and traveling in an arbitrary direction *r*. As the pulse travels through the nonlinear medium, the peak of the pulse travels slower than the leading and trailing edges due to the intensity dependent index of refraction.

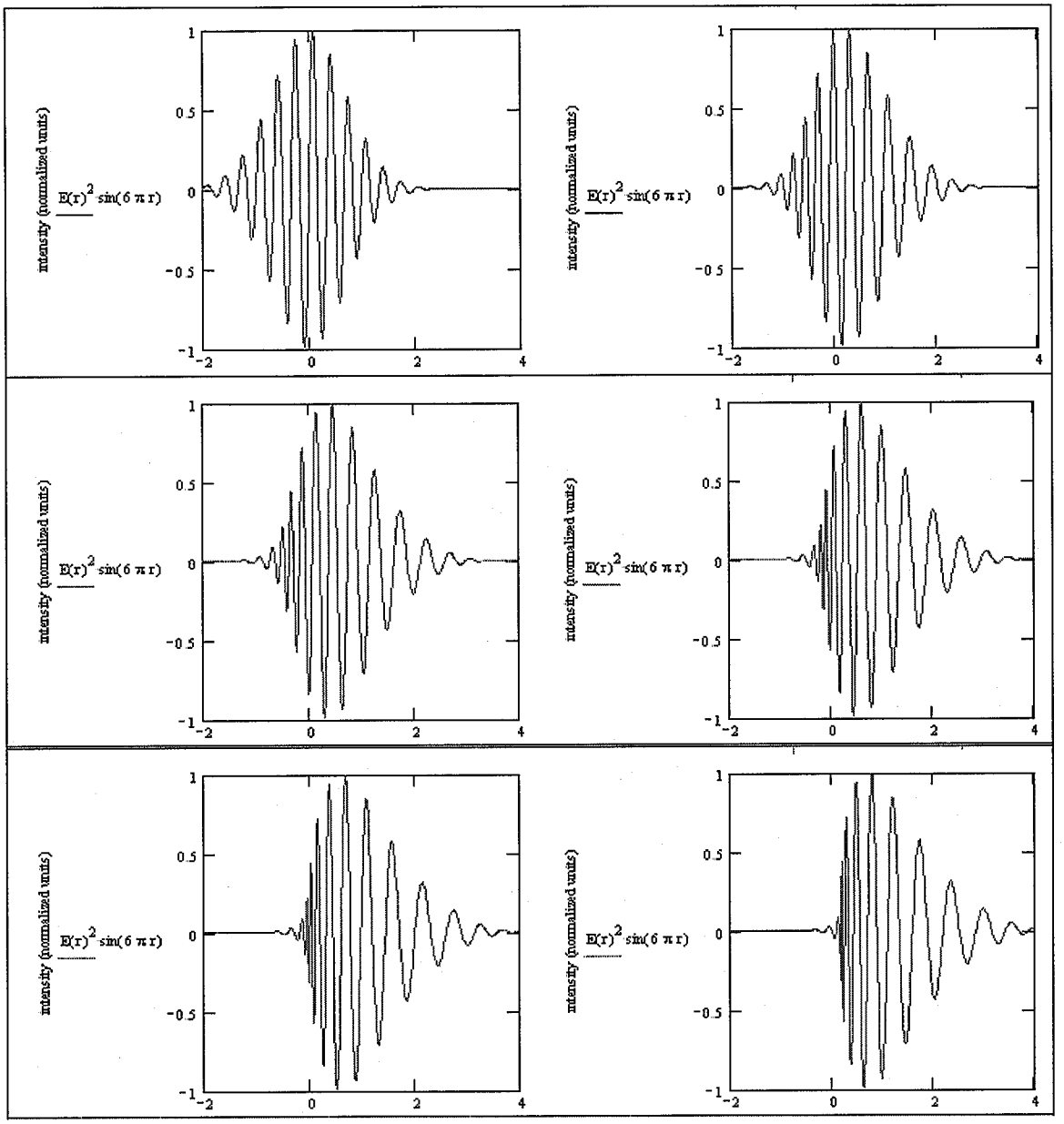

Figure 4: Gaussian pulse reshaping. These frames were created by multiplying the reshaped envelope by a sinusoidal function.

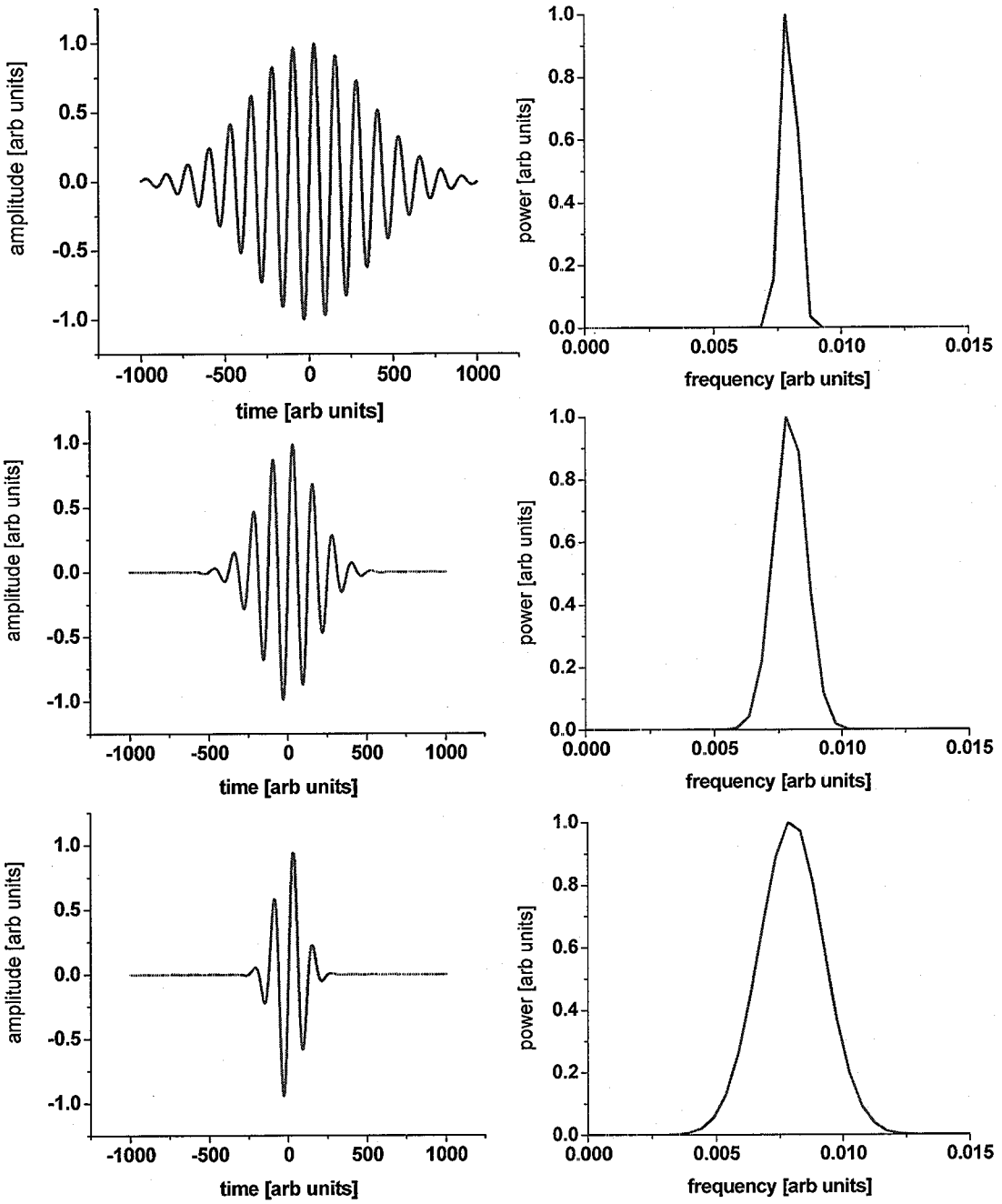

Figure 5: Fourier transform simulations. These plots show simulated Fourier frequency transforms for laser pulses of different time lengths. As the pulse gets shorter, its frequency spectrum gets broader.

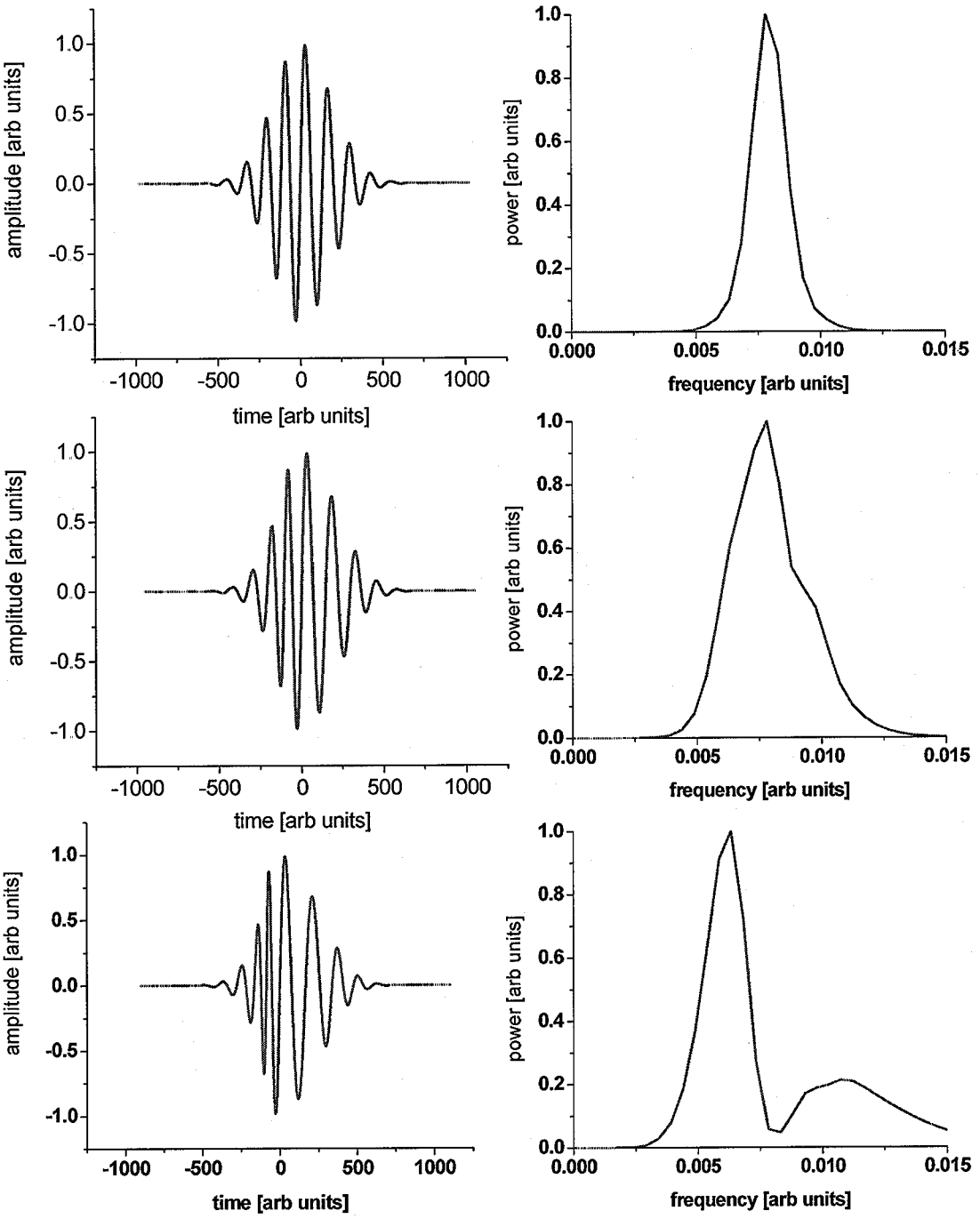

Figure 6: Fourier transform simulations. These images represent a laser pulse distorted in time by SPM. The more the pulse is distorted by traveling through a nonlinear medium, the wider its frequency spectrum.

Figure 7: Various fiber cleaving methods. Pictures taken with Motic digital camera. a) Standard fiber snapped by hand. b) Fiber cut with pair of scissors. c) Fiber cut with diamond tipped tool from FIS. d) Fiber cut using optical fiber cleaver from FITEL.

Figure 8: Fiber with score marks from the fiber stripping tool. These marks contribute to loss of light through the fiber.

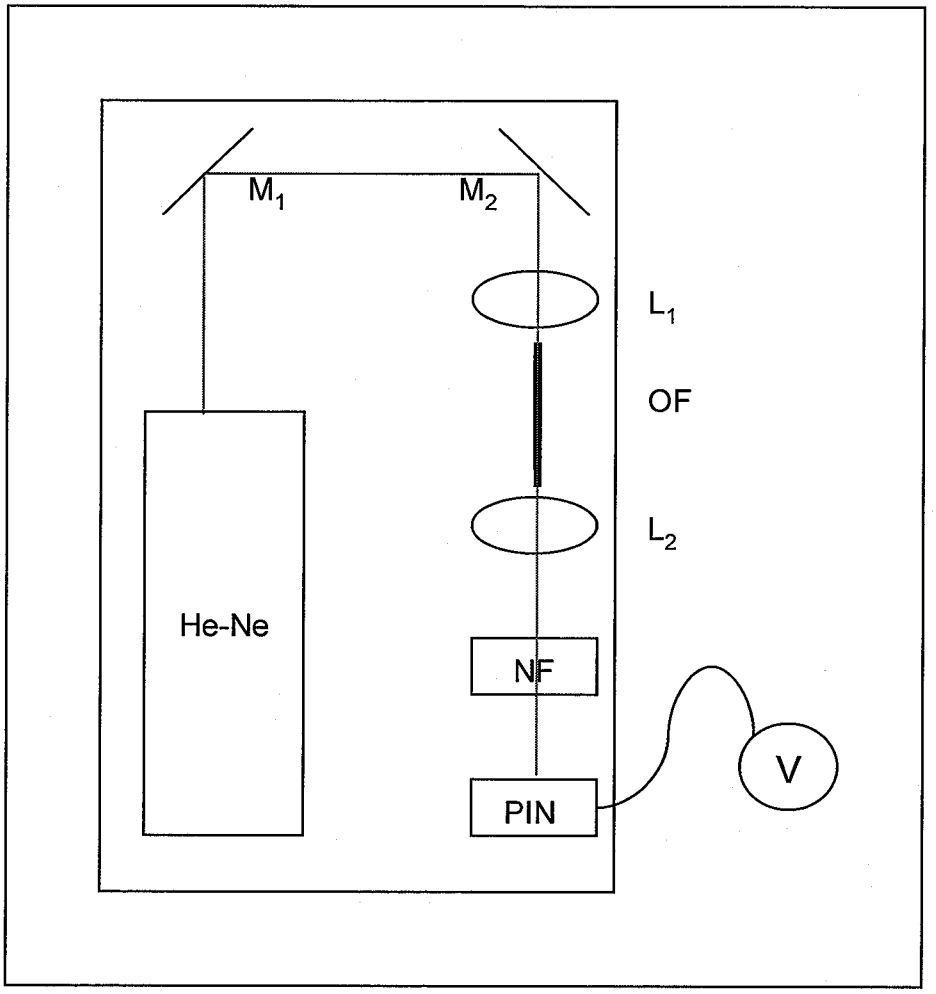

Figure 9: Initial Experimental Apparatus. He-Ne, Helium-Neon Laser; M, gold mirrors; L_1, aspheric lens with short focal length; OF, optical fiber; L_2, lens with long focal length; NF, neutral density filter; PIN, PIN-diode; V, digital multimeter.

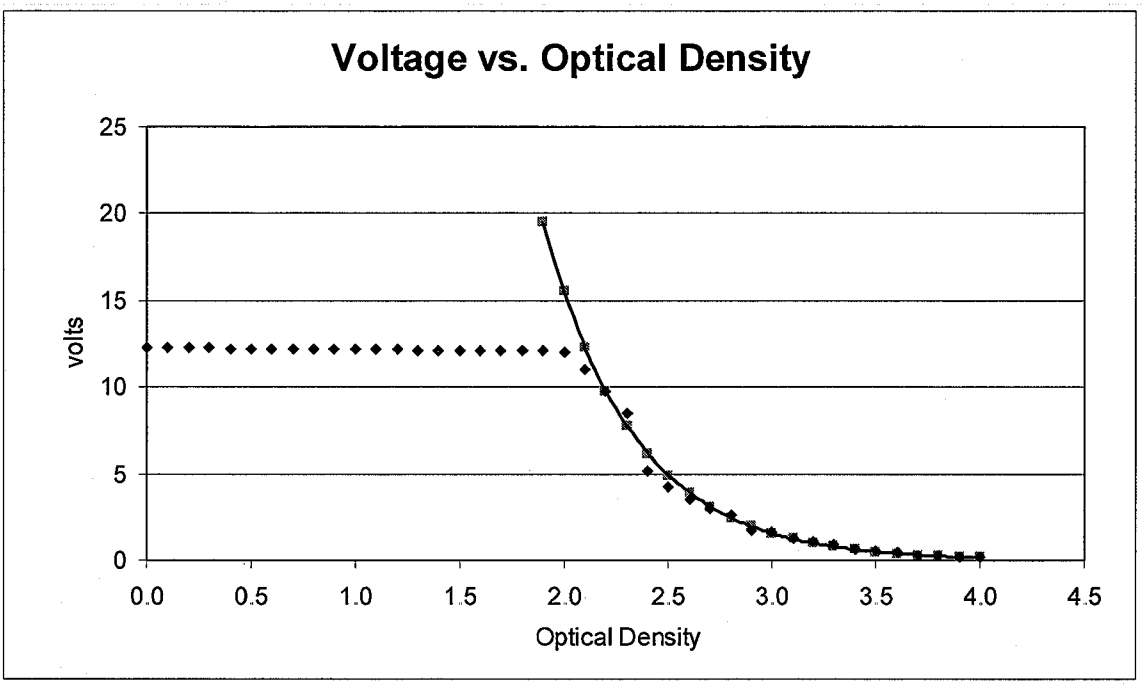

Figure 10: Voltage across PIN diode vs. optical density. This graph shows the measured voltages (blue) across the PIN diode from the He-Ne laser. The diode saturates at 12V. The pink points mark the extrapolated voltages and match the exponential fit shown in black.

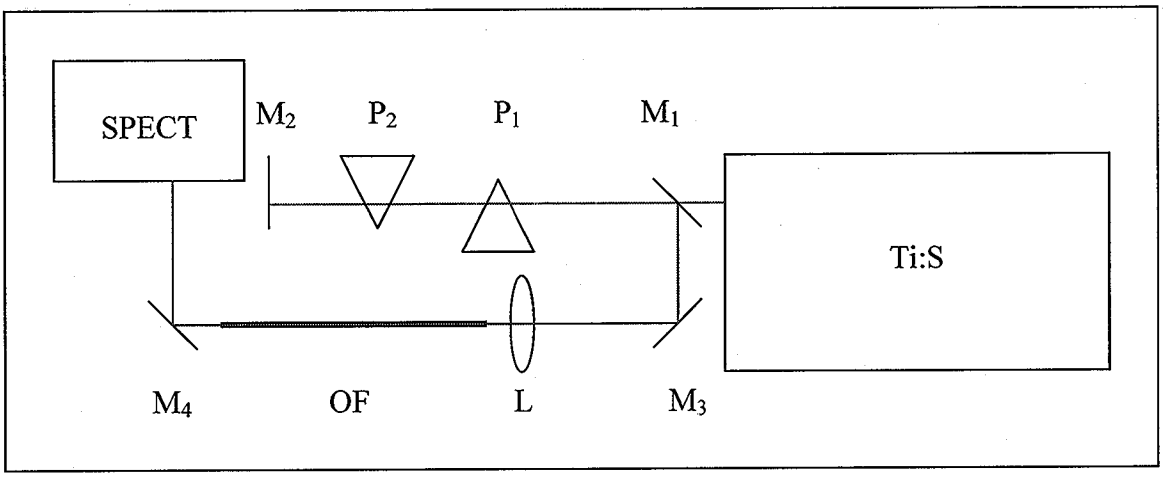

Figure 11: Diagram of actual apparatus. Ti:S, Titanium:sapphire Laser, M, gold mirror; P, prism; L, lens (f ~ 8mm); OF, optical fiber (L ~ 85cm); SPECT, spectrometer. The beam passes over the top of the first mirror and is directed down through the two prisms.

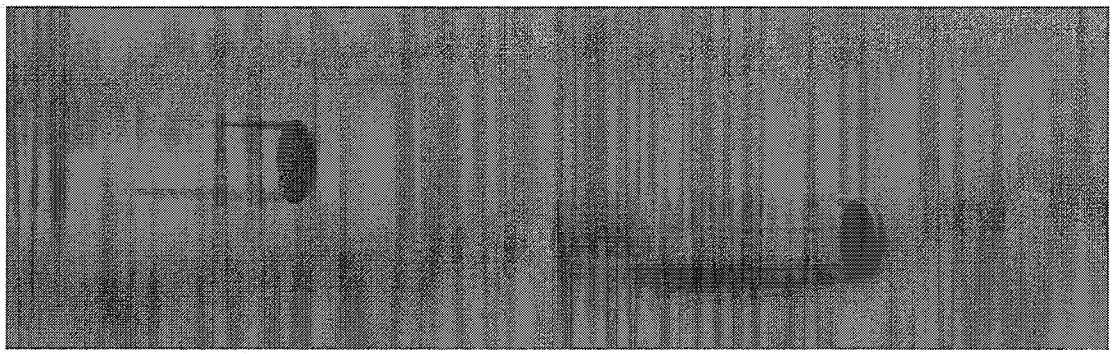

a b

Figure 12: Fiber used for experiment. a) Input face of fiber, b) output face.

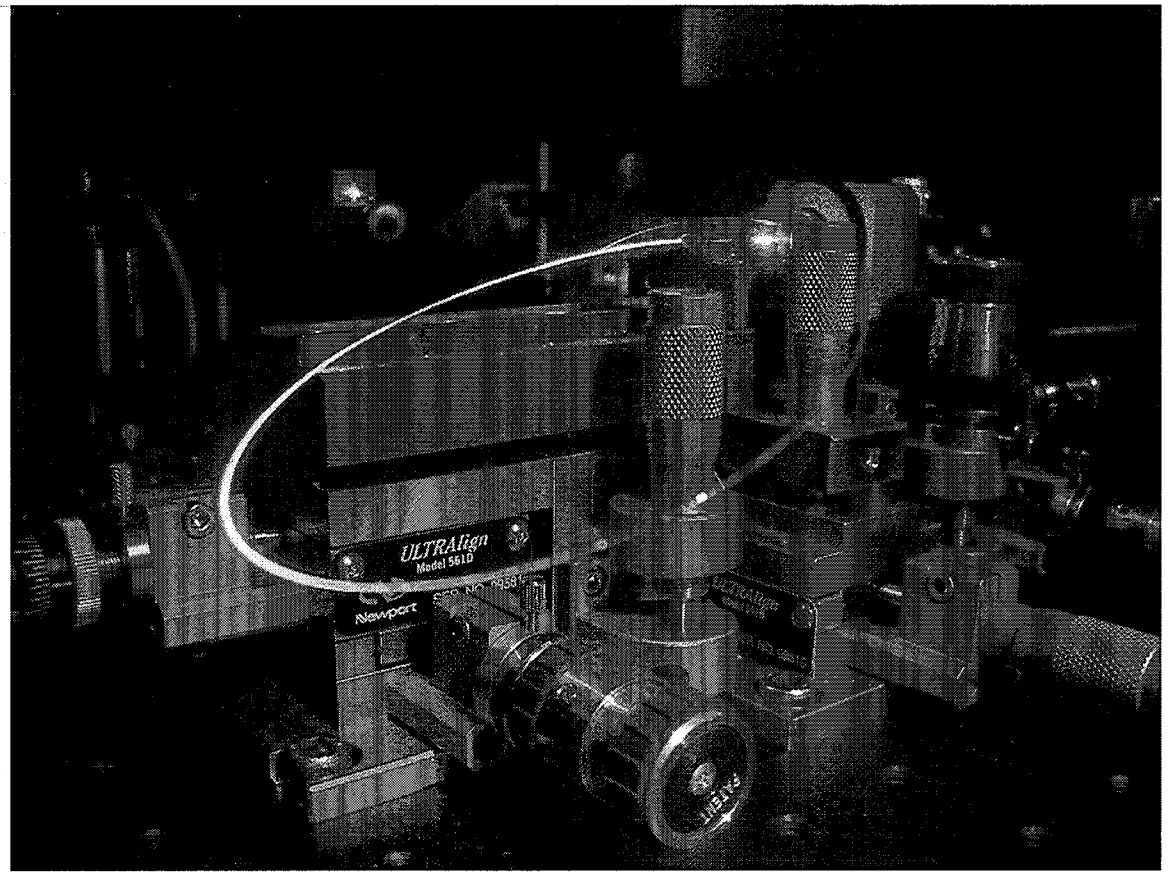

Figure 13: Light lost through bends of the fiber.

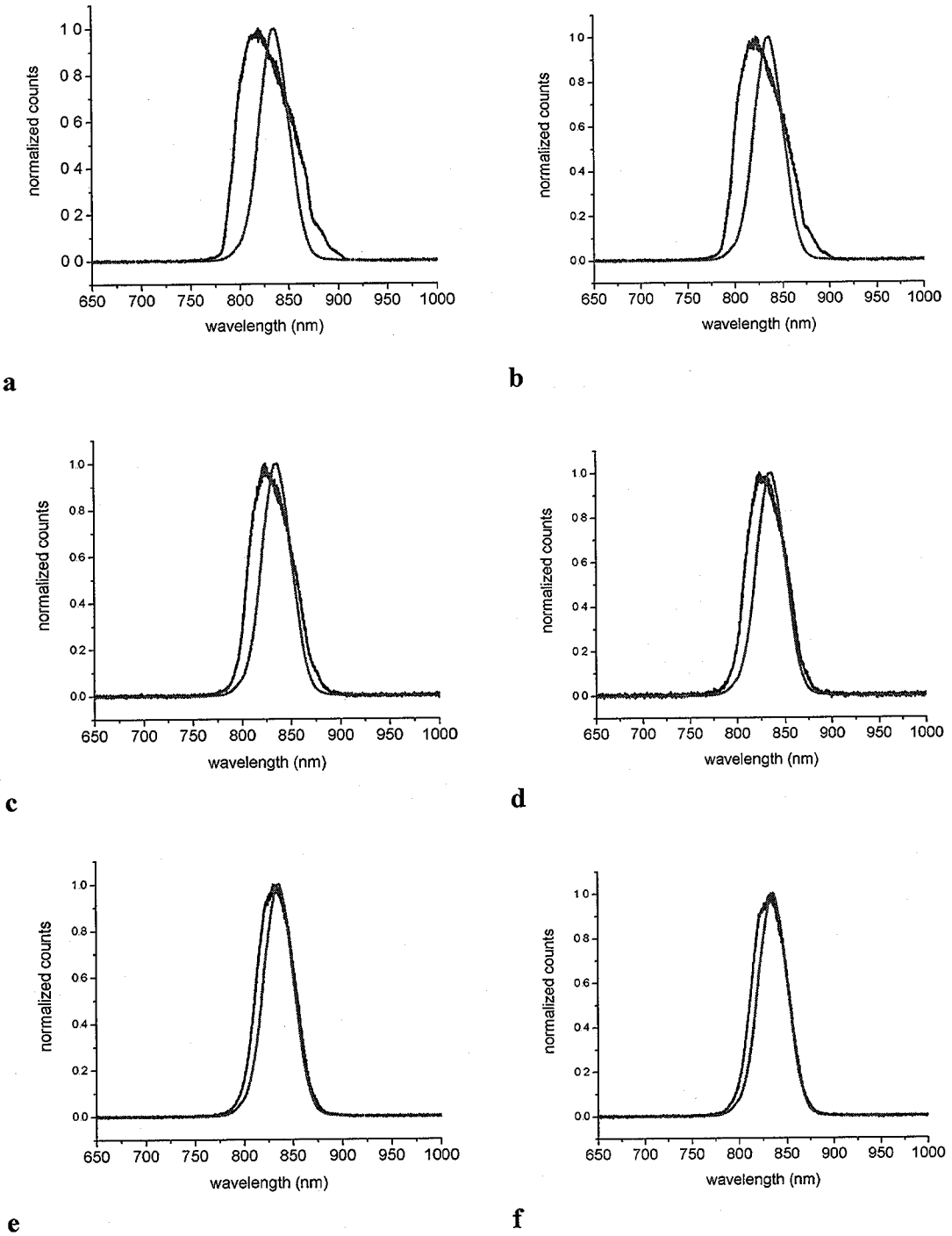

Figure 14: Output spectra for different levels of input power. The red line is the input spectra from the Ti:sapphire laser. The blue line shows the output spectra from the fiber. The levels of input power are: a) 380mW, b) 300mW, c) 160mW, d) 110mW, e) 63mW, f) 50mW.

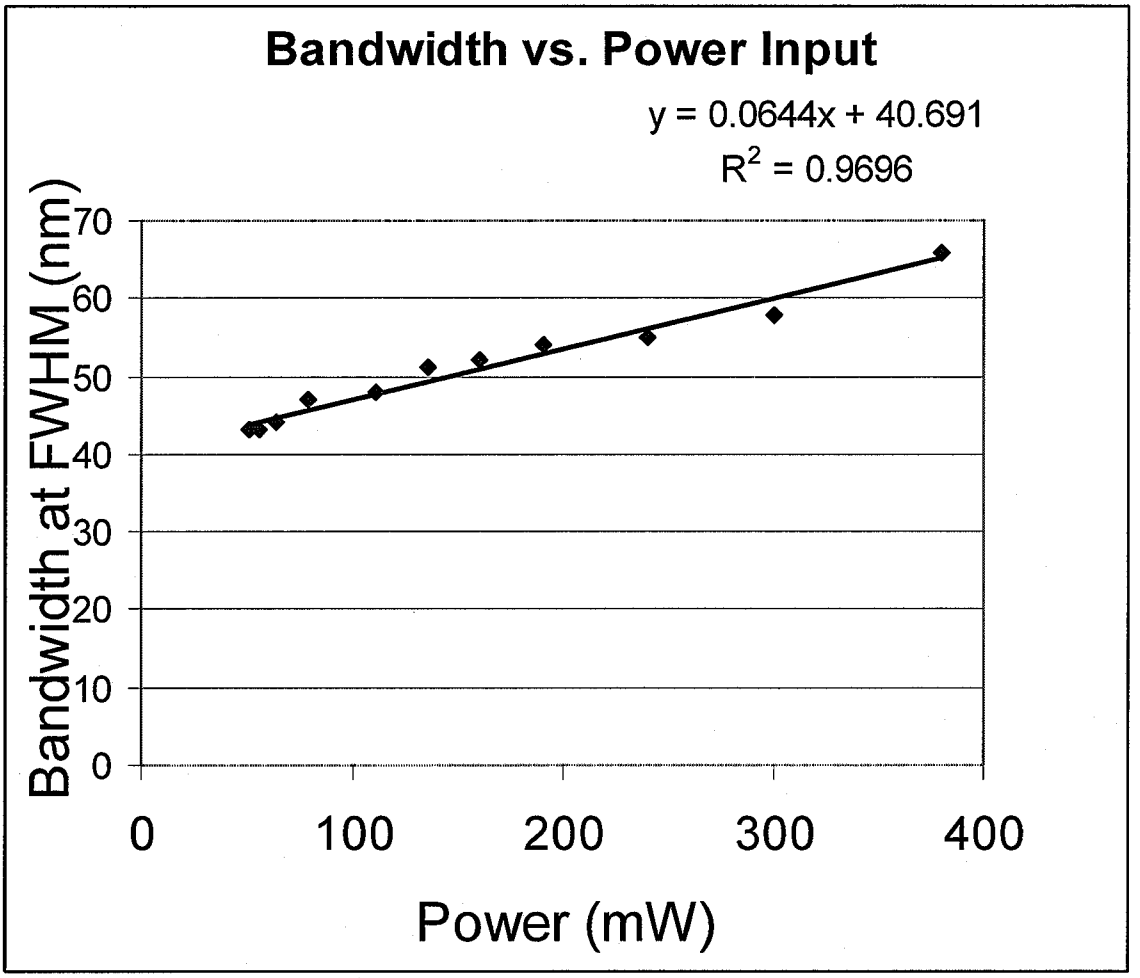

Figure 15: Output bandwidth as function of power. This graph shows the measured FWHM bandwidth for different power inputs.

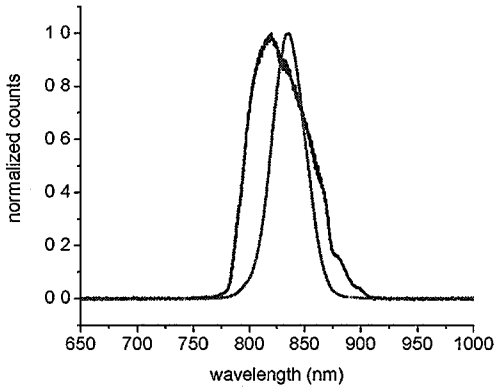

a

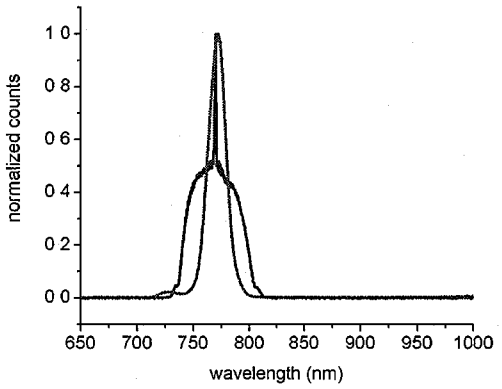

b

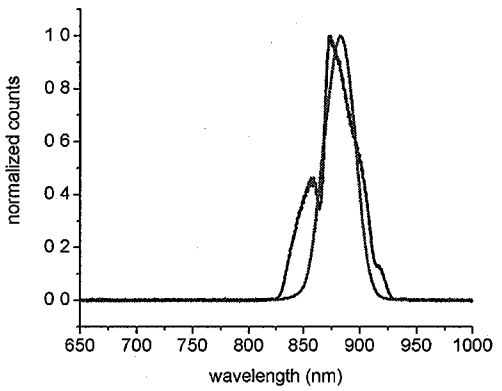

c

Figure 16: Output spectra as a function of input wavelength. a) Input spectrum centered at 835nm. b) Input spectrum centered at 770nm. c) Input spectrum centered at 882nm.